Molecular Vision 2016; 22:1503-1513 <http://www.molvis.org/molvis/v22/1503>
Received 16 September 2016 | Accepted 28 December 2016 | Published 30 December 2016

© 2016 Molecular Vision

Loss of Nrf2 exacerbates the visual deficits and optic neuritis elicited by experimental autoimmune encephalomyelitis

Chelsea M. Larabee,[1,2] Shruti Desai,[2] Agnieshka Agasing,[3] Constantin Georgescu,[3] Jonathan D. Wren,[3] Robert C. Axtell,[3] Scott M. Plafker[1,2]

[1]Oklahoma Center for Neuroscience, University of Oklahoma Health Sciences Center, Oklahoma City, OK; [2]Aging and Metabolism Research Program, Oklahoma Medical Research Foundation, Oklahoma City, OK; [3]Arthritis and Clinical Immunology Research Program, Oklahoma Medical Research Foundation, Oklahoma City, OK

Purpose: Optic neuritis, inflammation of the optic nerve, is experienced by most patients with multiple sclerosis (MS) and is typically characterized by episodes of acute, monocular vision loss. These episodes of inflammation can lead to damage or degeneration of the retinal ganglion cells (RGCs), the axons of which comprise the optic nerve. Experimental autoimmune encephalomyelitis (EAE) is a well-established model of MS in which mice are immunized to produce a neuroautoimmunity that recapitulates the cardinal hallmarks of human disease, namely, inflammation, demyelination, and neurodegeneration of the brain, spinal cord, and optic nerve. Inflammation-associated oxidative stress plays a key role in promoting spinal cord damage in EAE. However, the role of oxidative stress in optic neuritis and the associated visual deficits has not been studied. To address this gap in research, we sought to determine how a deficiency in the master antioxidant transcription factor (using nuclear factor-E2-related factor [Nrf2]-deficient mice) affects visual pathology in the EAE model.

Methods: EAE was induced in 8-week-old wild-type (WT) and Nrf2 knockout (KO) mice by immunization against the myelin oligodendrocyte glycoprotein (MOG) peptide antigen. Motor deficits were monitored daily, as was visual acuity using the established functional optokinetic tracking (OKT) assay. Mice were euthanized 21 days post-immunization for histological analyses. The optic nerves were paraffin-embedded and stained with hematoxylin and eosin (H&E) or immune cell type–specific antibodies to analyze inflammatory infiltrates. The retinas were flatmounted and stained with an RGC-specific antibody, and the RGCs were counted to assess neurodegeneration. T-helper (Th) cell-associated cytokines were measured in spleens with enzyme-linked immunosorbent assay (ELISA). Immune analyses of healthy, non-EAE mice were characterized with flow cytometry to assess the baseline immune cell profiles.

Results: Female Nrf2 KO mice exhibited more severe EAE-induced motor deficits compared with female WT mice. In both genders, EAE elicited more severe visual acuity deficits, inflammation of the optic nerve, and RGC degeneration in KO mice compared with their strain- and age-matched WT counterparts. Visual acuity deficits were primarily present in (and only exacerbated in) one eye of each mouse. Excess inflammatory cells within the optic nerves of the KO mice were primarily comprised of T-cells, and greater RGC degeneration in the KO mice was most prevalent in the central retina compared with the peripheral retina. Nrf2 KO spleens exhibited an increased Th1- but not Th17-associated immune response. This enhanced pathology in the KO mice was not due to global differences in immune system development between the two genotypes.

Conclusions: This is the first study to report that genetic ablation of Nrf2 exacerbates visual deficits, inflammation of the optic nerve, and RGC degeneration in a murine model of MS, suggesting that Nrf2 plays a neuro- and cytoprotective role in EAE-associated optic neuritis.

Optic neuritis (ON), inflammation of the optic nerve, occurs in more than 50% of multiple sclerosis (MS) cases and is the presenting symptom in 19% of MS diagnoses [1]. ON is characterized by acute, unilateral episodes of deficits in central visual acuity, color vision, visual field size, and afferent pupillary function [2]. Functional prognosis is promising for ON episodes in earlier stages of MS, as most patients fully recover visual function, despite the significant neurodegeneration of the cells that comprise the optic nerve, called retinal ganglion cells (RGCs) [3]. However, in later more progressive stages of MS, severe RGC loss is correlated with permanent decreases in visual acuity, contrast, and field size [4].

Experimental autoimmune encephalomyelitis (EAE) is a well-established animal model of MS that recapitulates the common hallmarks in human disease, namely, inflammation of the central nervous system (CNS), demyelination, oxidative stress, and neurodegeneration [5,6]. EAE is induced by immunization against a myelin-specific antigen to recapitulate the demyelinating autoimmunity in MS. We and others

Correspondence to: Scott M Plafker, Aging and Metabolism Research Program, Oklahoma Medical Research Foundation, 825 NE 13th St, OKC, OK 73104, Phone: (405) 271-1735; FAX: (405) 271-1437; email: PlafkerS@omrf.org

have established that the murine EAE model exhibits visual pathology reminiscent of ON in MS, such as episodic visual acuity loss, inflammation of the optic nerve, and RGC degeneration [6-8].

Nuclear factor-E2-related factor (Nrf2) is a redox-regulated transcription factor that orchestrates the expression of a battery of antioxidant and cytoprotective genes [9]. Nrf2 is a known target of the U.S. Food and Drug Administration (FDA)–approved treatment for MS, dimethyl fumarate (DMF) [10], and the Nrf2-activator sulforaphane ameliorates EAE-elicited motor deficits [6]. These findings are consistent with the well-established role of oxidative stress in MS pathogenesis of the brain and the spinal cord [11]. In the work reported here, we have undertaken a detailed analysis of the contribution of Nrf2 to optic neuritis and the visual deficits and pathology that accompany EAE. Our data show that in response to EAE, mice deficient for Nrf2 exhibit exacerbated visual acuity deficits, inflammation of the optic nerve, and retinal degeneration. The inflammation of the optic nerve primarily consists of T-cells, and RGCs are primarily lost in the central retina. Although baseline immune-cell profiles before EAE challenge are similar regardless of Nrf2 status, Nrf2 KO mice exhibit a greater T-helper 1-associated splenic response.

METHODS

Mice: All animal care was performed in compliance with the protocol approved by the Oklahoma Medical Research Foundation Institutional Animal Care and Use Committee and adhered to the ARVO Statement for Use of Animals in Research. $Nrf2^{-/-}$ and $Nrf2^{+/+}$ mice (previously characterized in [12,13]) were originally generated in a 129SVJ background and backcrossed into C57BL/6J for greater than ten generations. These lines were subsequently crossed with C57BL/6J-Tg(CAG-Cox8/EGFP)49Rin, a strain that transgenically expresses a mitochondria-targeted green fluorescent protein (GFP). However, we exclusively used experimental mice that were negative for the GFP transgene. The mice were euthanized at approximately 11 weeks of age with CO_2 asphyxiation followed by PBS (1X PBS: 137 mM NaCl, 2.7 mM KCl, 10 mM Na_2HPO_4, 1.8 mM KH_2PO_4, pH 7.5.) cardiac perfusion.

Induction of EAE: Eight- to nine-week-old mice were immunized subcutaneously with 150 µg myelin oligodendrocyte glycoprotein ($MOG_{35–55}$; Bio-Synthesis, City, TX) emulsified in complete Freund's adjuvant (CFA; Difco Laboratories, Detroit, MI) containing 2.5 mg/ml heat-killed *Myobacterium tuberculosis*. Mice were injected intraperitoneally with 250 ng *Bordetella pertussis* toxin (Chondrex, Redmond, WA) the day of, and 2 days following, $MOG_{35–55}$ immunization. At 21 days post-immunization, the mice were euthanized for the histological analyses. EAE clinical manifestations of progressive ascending paralysis were assessed daily using a standard scoring system: 1 = loss of tail tone, 2 = hind limb paresis, 3 = complete hind limb paralysis, 4 = hind limb paralysis and forelimb paresis, and 5 = moribund or dead. Mice were weighed daily to ensure weight loss did not exceed 25% of starting weight. All EAE data were gathered in two independent experiments from cohorts of the same 12 WT mice and ten KO mice.

Visual acuity assessment: Visual acuity threshold was measured daily with the optokinetic tracking (OKT) response using Optometry software and apparatus (Cerebral Mechanics Inc., Alberta, Canada) as previously described [7,14]. Briefly, mice were surrounded by a virtual cylinder consisting of vertical lines rotating at varying frequencies, and tracking behavior was assessed by an investigator blinded to genotype. Visual acuity is represented as the highest spatial frequency at which mice track the rotating cylinder. Because tracking is a temporal to nasal-specific reflex, counter-clockwise and clockwise rotations exclusively test the right eye and the left eye, respectively. Occasionally, the mice were too unsteady due to motor deficits to adequately perform OKT analysis, in which case a measurement was not recorded for that mouse on that day.

H&E analysis of the optic nerve: Optic nerve tissue was prepared and stained as previously described [7]. Briefly, after CO_2 asphyxiation and cardiac perfusion with PBS, the optic nerves were fixed in 10% neutral buffered formalin (NBF) for 2.5–6.5 h before processing, paraffin-embedding, and sectioning into 5 µm longitudinal sections. Two slides per optic nerve, corresponding to the lateral and medial longitudinal planes, were deparaffinized and stained with hematoxylin and eosin (H&E; described in [7]), and the inflammation scores were averaged from the two sections. The images of the nerves were graded for inflammation by a blinded investigator according to the following scale: 0 = absent or minimal infiltration, 1 = moderate infiltration throughout, 2 = moderate infiltration with areas of severe infiltration, and 3 = severe infiltration throughout.

Immunohistochemistry of the optic nerve: Two slides per nerve (neighboring H&E-analyzed slides) were immunohistochemically stained with cell type–specific antibodies as previously described [7]. Briefly, following deparaffinization and antigen retrieval, slides were incubated in blocking solution (10% goat serum + 3% bovine serum albumin [BSA] in PBS) followed by overnight incubation in primary antibody at 4 °C. The following day, slides were

washed in PBS, incubated for 1 h in fluorescent-conjugated secondary antibody (Alexa$_{488/546/647}$nm Fluor-conjugated goat anti-rat/mouse/rabbit immunoglobulin G [IgG; Molecular Probes, Eugene, OR; 1:500]) and Hoechst 33342 (2 µg/ml), and washed again before coverslipping. The cell type–specific primary antibodies used were anti-B220 (B-cells; BioLegend, San Diego, CA, cat# 103201; 1:400), anti-CD3 (T-cells; Abcam, Cambridge, MA, cat# ab5690; 1:250), anti-Iba1 (macrophages and microglia; Millipore, Darmstadt, Germany, cat# MABN92; 1:50), and anti-CNPase (myelin; Covance, Princeton, NJ, cat# SMI-91R; 1:500). Separate grayscale images for each channel were captured using NIS-Elements software (Nikon, Tokyo, Japan), and representative images were processed in Adobe Photoshop (Version 8.0, San Jose, CA). Analysis was performed on raw images using NIH ImageJ software. B220- or CD4-positive cells were counted in three representative fields (each normalized to the nerve area) throughout each of the two sections (for a total of six representative fields per nerve) and are represented as the average number of cells normalized to the area. Due to diffuse staining patterns, the Iba1- and CNPase-positive cells are represented as the average percentage area stained in three representative fields throughout each of the two sections (for a total of six fields).

Flatmount analysis of the retina: Eyes were enucleated in 10% NBF and fixed for 4–7.5 h before the retinas were isolated under a dissecting microscope (Olympus SZ-PT, Center Valley, PA) followed by permeabilization in 1% Triton X-100/PBS for approximately 30 min. The retinas were then incubated for approximately 2 h in blocking solution (10% donkey serum + 3% BSA in PBS) and then incubated overnight in the RGC-specific antibody anti-Brn3a (goat; Santa Cruz Biotechnology, Santa Cruz, CA; sc31984; 1:500) diluted in blocking solution at 4 °C. The following day, the retinas were washed in PBS, cut to lie flat under a dissecting microscope, and incubated with Alexa$_{488nm}$ Fluor-conjugated donkey anti-goat IgG (Molecular Probes; 1:1,000) and Hoechst 33342 (2 µg/ml) in 3% BSA/PBS for 1 h. The retinas were then washed in PBS before they were mounted with Prolong Gold mounting medium (Life Technologies, Grand Island, NY). The retinas were examined with a Nikon 80i microscope with a 20× objective, and images were captured using a DXM1200C camera using NIS-Elements software (Nikon). The central retina was more populated with RGCs than the peripheral retina, and the flatmounts consisted of four quadrants; therefore, a representative image was captured from the peripheral, medial, and central retina within each quadrant, for a total of 12 pictures per retina. Images were cropped to 325 µm^2 and contrast-enhanced in Adobe Photoshop 8.0. Using NIH ImageJ software, the manipulated images were subjected to a user-defined threshold such that only the Brn3a-positive areas were represented, and the "Analyze particles" function was used to count individual regions of interest (RGCs).

Flow cytometry: Following CO_2 asphyxiation and cervical dislocation, the spleen, thymus, and hind limb bone marrow were collected and manually dissociated on ice in FACS buffer (2% FCS in PBS). Cell suspensions were spun down at 4 °C before resuspension in primary antibodies at 1:200 in FACS buffer for 15 min. The following primary-conjugated antibodies were used: anti-CD3 (T-cells; eBioscience, San Diego, CA; clone 145–2C11), anti-CD4 (T-helper cells; BioLegend; clone RM4–5), anti-CD8 (cytotoxic T-cells; Becton, Dickinson, and Co, Franklin Lakes, NJ; clone 53–67), anti-Cd11b (macrophages; BioLegend; clone M1/70), anti-Gr-1 (granulocytes; eBioscience; clone RB6–8C5), and anti-CD19 (B-cells; eBioscience; clone 103). Following the FACS buffer wash, the samples were run on an LSRII (Becton, Dickinson, and Co) running Diva version 8 software, and the data were analyzed using FlowJo vX.0.7 software (Ashland, OR).

ELISA: Spleens from the EAE WT and Nrf2 KO mice were harvested and mechanically disrupted to obtain single cell suspensions. Cells (2.5×10^6/ml) were stimulated with $MOG_{35–55}$ (10 µg/ml) for 72 h in complete Roswell Park Memorial Institute (RPMI) 1640 (Gibco, Paisley, UK). Following culture, the cells were spun down, and supernatants were collected for enzyme-linked immunosorbent assay (ELISA). Following the manufacturer's instructions, the concentrations of interleukin-6 (IL-6), IL-17, and interferon-gamma (IFN-γ) were determined using anti-mouse ELISA kits (R&D Systems, Minneapolis, MN).

Statistical analysis: Confidence intervals and p values for the statistical significance of each studied effect in the longitudinal or binocular data were determined by fitting the data to a linear mixed-effects model, using the lme function implemented in the nlme R package. This function is an extended version of regular linear regression but can accommodate complex data collection design features, such as longitudinal measurements, nested layers, and within-group correlation. The method formulation [15], computational method [16], and implementation of the model in R [17] have previously been described. Proper handling of the multilayer embedded data collection design was achieved by correct specification of the random effect structure in the corresponding parameter of the lme function (mouse/eye for the longitudinal OKT data and mouse/eye/eye region for the RGC analyses). Fixed-effect coefficient tables were extracted with the table method, and confidence intervals were returned by the intervals function in the nlme package. Standard testing methods, such as ANOVA with appropriate post hoc analyses, the Student *t*

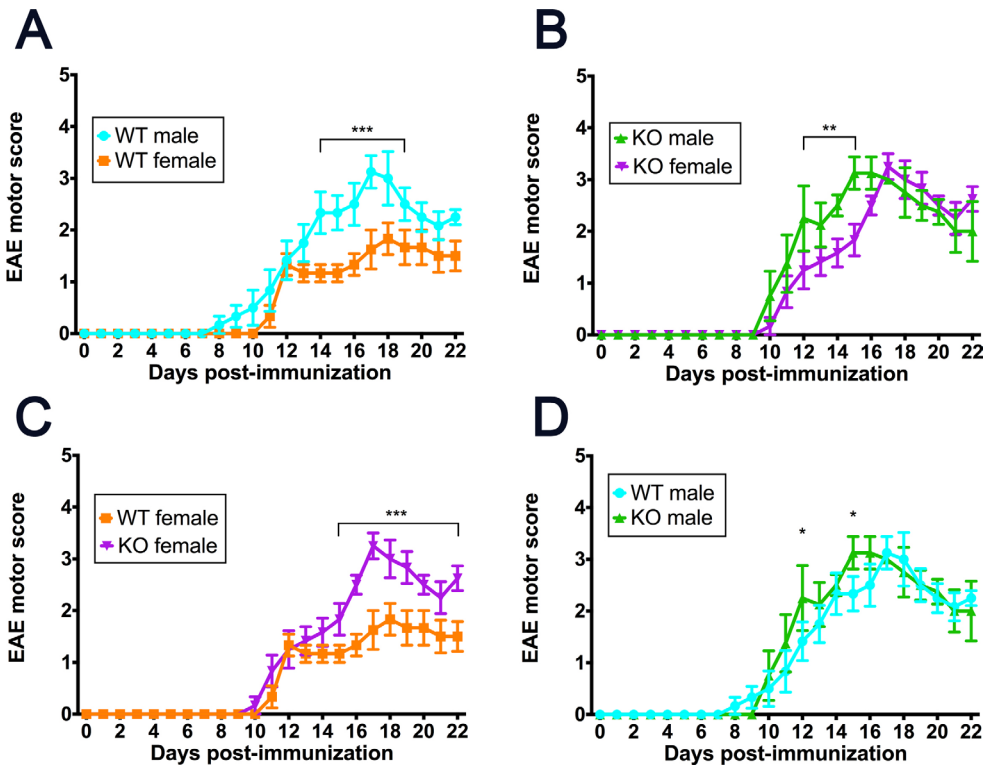

Figure 1. Nrf2-deficient female mice exhibited more severe EAE-associated motor deficits compared with the wild-type mice. **A**–**D**: Daily mean experimental autoimmune encephalomyelitis (EAE) motor severity scores for wild-type (WT) male mice (aqua circles), WT female mice (orange squares), knockout (KO) male mice (green triangles), and KO female mice (purple upside-down triangles). Error bars represent the standard error of the mean (SEM); n = 4–6 mice per genotype per gender pooled from two independent experiments. *p<0.05, **p<0.005, ***p<0.001 by the linear mixed-effects model.

test, the Mann–Whitney exact test, or linear regression, were employed when no embedding was involved.

RESULTS

It was previously established that Nrf2-knockout (KO) mice exhibit exacerbated motor deficits in response to EAE compared with wild-type (WT) control mice [18]. The purpose of this study was to determine if this Nrf2-dependent disease exacerbation extends to visual dysfunction. Functional visual acuity was assessed with OKT analysis, and histological analyses were used to assess inflammation of the optic nerve and neurodegeneration.

Nrf2-deficient mice exhibit exacerbated EAE-induced paralysis in a sex-dependent manner: EAE was induced in the Nrf2 KO and strain-, age-, and sex-matched WT control mice, and motor deficits were monitored daily. The male WT mice exhibited more severe motor disease compared with the WT female mice (Figure 1A). In contrast, the KO male mice exhibited modestly increased kinetics of motor deficit onset compared with the KO female mice, but the severity of the disease did not differ between the KO genders (Figure 1B). Due to this notable gender difference in the WT mice, we analyzed the effect of the absence of Nrf2 in EAE paralysis within each gender (Figure 1C,D). Consistent with Johnson et al. [18], the KO female mice exhibited statistically significantly exacerbated motor symptoms compared with the WT female mice (Figure 1C). However, the absence of Nrf2 had less of an impact on the severity of paralysis exhibited by male mice, reaching statistical significance on only 2 days (Figure 1D).

The baseline immune profiles between healthy WT and Nrf2 KO mice are comparable: To eliminate the possibility that this differential response to EAE is attributable to developmental differences in baseline immune cell profiles based on the presence or absence of Nrf2, we used flow cytometry with antibodies against various immune cell types to analyze the immune organs of healthy, non-EAE WT and Nrf2 KO mice (Figure 2A–C). No differences in the thymus T-cell populations ($CD4^+$, $CD8^+$, and $CD4^+CD8^+$) were detected (Figure 2A). We also quantitated the presence of $CD4^+$ T-cells, $CD8^+$ T-cells, $Gr\text{-}1^+$ granulocytes, $Iba1^+$ macrophages/microglia, and $CD19^+$ B-cells in the bone marrow and the spleen (Figure 2B,C). Only minor differences were observed in the levels of the bone marrow B-cells (Figure 2B) and the splenic $CD4^+$ T-cells (Figure 2C). Overall, these data support the notion that the differences observed between KO and WT mice in response to EAE are likely not solely attributable to developmental differences between general immune cell populations, especially considering that these immune cell populations are lower in the KO mice.

Th1 cytokines differ between Nrf2-deficient and wild-type mice spleens during EAE: T-helper (Th) 1 and Th17 cells are involved in MS and EAE pathogenesis, and the ratio of these two cell types affects disease severity and treatment efficacy [19]. Twenty-one days post-immunization (DPI), spleens were harvested from the EAE mice and analyzed with ELISA for the presence of the Th17-associated cytokines, IL-6 (Figure 2D) and IL-17 (Figure 2E), as well as Th1-associated cytokine IFN-γ (Figure 2F). The EAE-challenged spleens from the Nrf2 KO mice expressed statistically significantly more IFN-γ compared with the spleens from the WT mice (Figure 2F), but no differences in either of the Th17-associated cytokines were detected (Figure 2D,E). Note that the results for the male and female mice within the same genotype did not differ statistically significantly for any cytokines as analyzed with the unpaired Student *t* test. These data indicate that the secretory profiles of the T-cells recruited in EAE differ between WT and Nrf2 KO mice.

Absence of Nrf2 exacerbates EAE-induced monocular visual acuity impairment: We conducted a series of experiments using OKT to interrogate the consequences of Nrf2 loss on EAE-induced visual deficits. The data were binned to analyze for sex and genotype differences. Regardless of genotype and sex, EAE induced by myelin-immunization elicits acute, asymmetric episodes of visual acuity loss that coincide with the onset of motor disease (Figure 3A,B), identical to the pattern of vision loss we previously reported in EAE induced by the transfer of myelin-specific T-cells [7] (represented in Figure 3A). Mice of both genotypes exhibited asymmetric deficits (Figure 3B) such that the large majority of mice had an eye that exhibited more severe deficits in visual acuity (termed the more affected eye [MA]; Figure 3C,D,G) and an eye with much less or no vision loss (termed the less affected eye [LA]; Figure 3E,F,H). Interestingly, in contrast to the motor deficit patterns, EAE-induced visual impairment in the WT mice is not sexually dimorphic (Figure 3C,E), as there was only a modest difference in the LA eyes at 18 and 19 DPI. Likewise, although the KO mice exhibited statistically significant differences in the LA and MA eyes when the male mice were compared to the female mice, these differences were modest (Figure 3D,F). As a consequence, all subsequent data are presented with the male and female mice combined

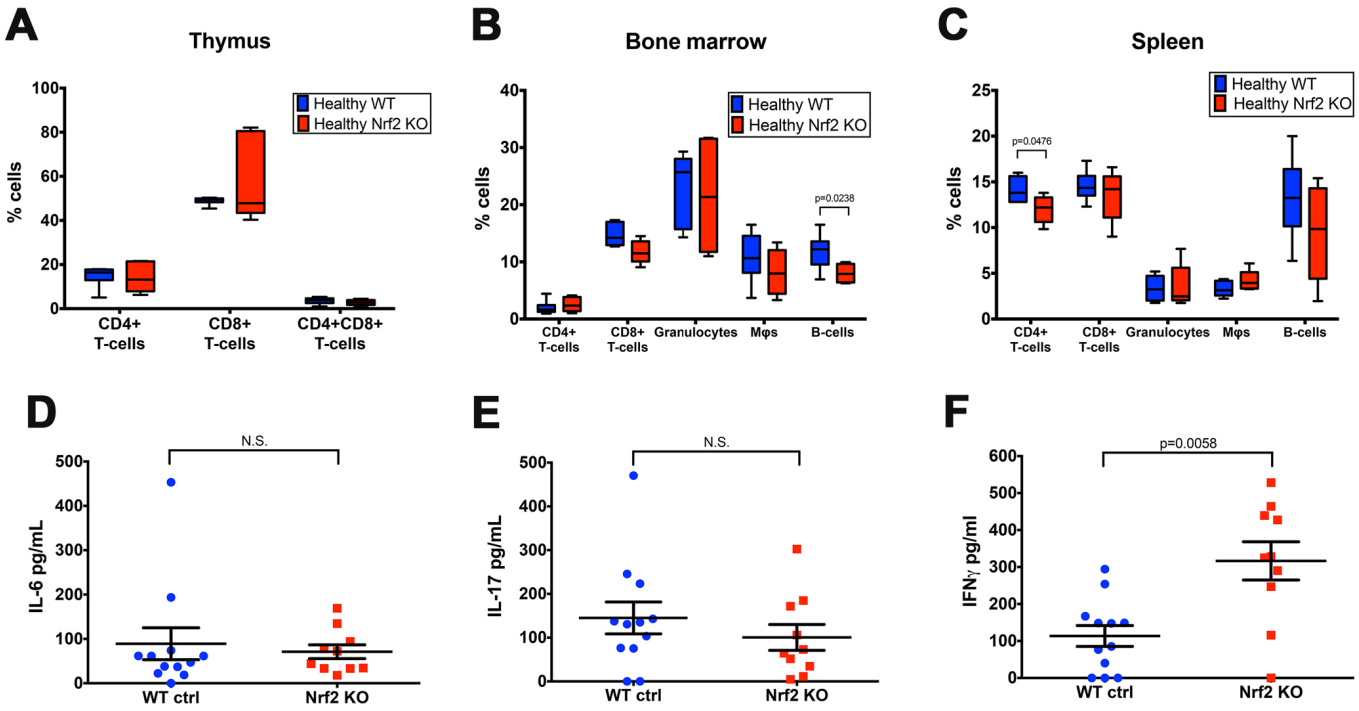

Figure 2. Nrf2-deficient and wild-type mice exhibit different immune responses to EAE despite comparable immune cell profiles before EAE challenge. Flow cytometric analysis of cells recovered from the thymus (**A**), bone marrow (**B**), and spleen (**C**) of healthy, non-experimental autoimmune encephalomyelitis (EAE) wild-type (WT; blue, left) and nuclear factor-E2-related factor (Nrf2) knockout (KO; red, right) mice. The antibodies used detected $CD4^+$ T-cells, $CD8^+$ T-cells, $CD4^+CD8^+$ T-cells (**A**), $Gr\text{-}1^+$ granulocytes (**B**, **C**), $Iba1^+$ macrophages (**B**, **C**), and $CD19^+$ B-cells (**B**, **C**). Whiskers indicate min/max. n = 6 (three male mice, three female mice) per group. Mann–Whitney analysis. **D**–**F**: ELISA analysis of WT (blue circles) and Nrf2 KO (red squares) EAE spleens to determine the interleukin-6 (IL-6; **D**), IL-17 (**E**), and interferon-gamma (IFN-γ; **F**) cytokine levels. n = 10–12. Mann-Whitney was used for statistical analysis.

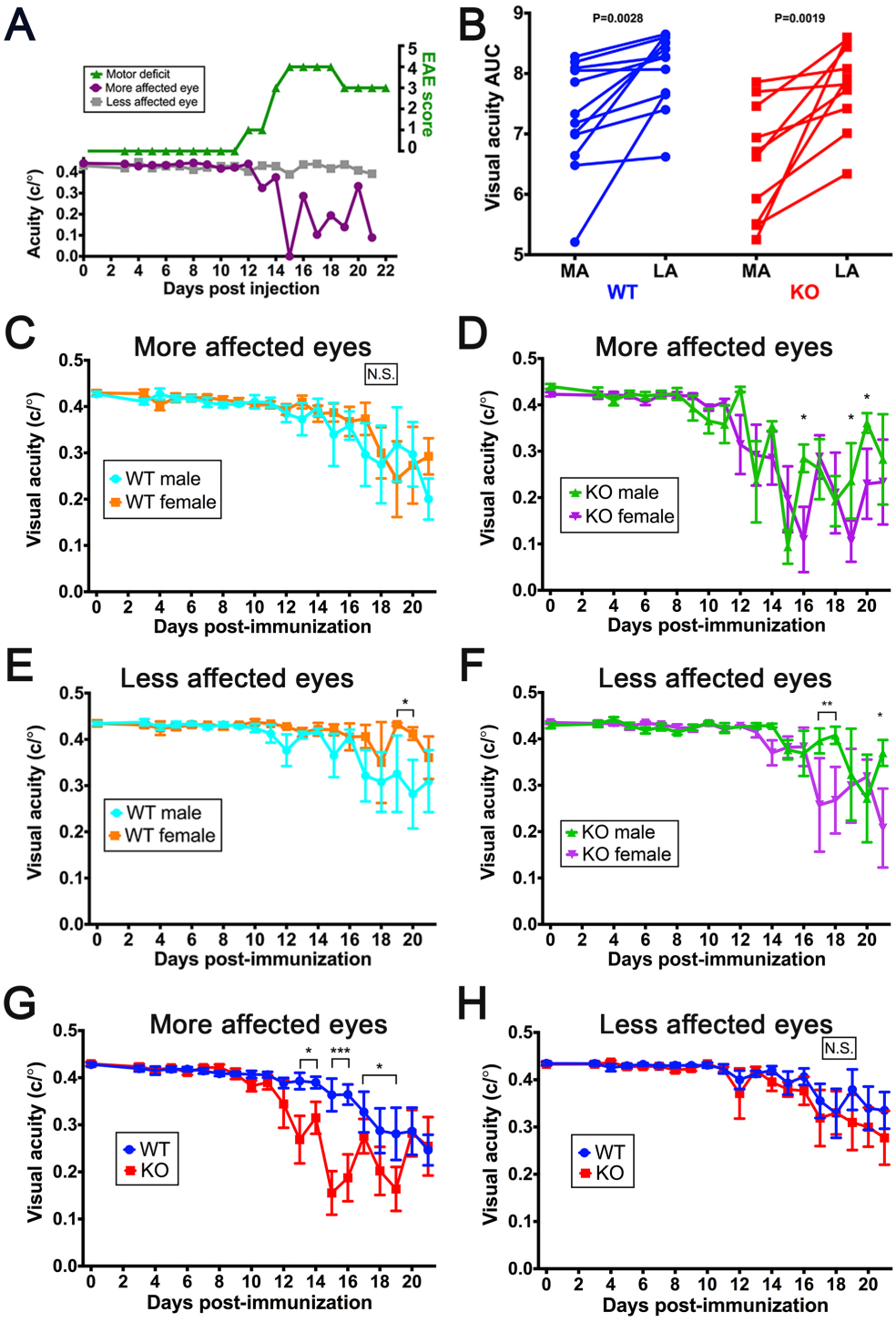

Figure 3. Nrf2-deficient mice exhibit more severe EAE-associated monocular visual acuity deficits. **A**: Representative time course of acute, monocular episodes of deficits in visual acuity as measured with optokinetic tracking (OKT) of an experimental autoimmune encephalomyelitis (EAE) mouse. The more affected (MA) eye (purple circles) deficits coincide with the onset of motor deficits (green triangles), whereas the less affected (LA) eye (gray squares) does not exhibit substantial acuity loss. **B**: Area under the curve (AUC) of visual acuity values (cycles per degree) throughout the experiment for the MA and LA eyes of wild-type (WT; blue circles) and knockout (KO; red squares) EAE mice in which two eyes from the same mouse are connected by a line. n = 10–12 mice. Two-tailed paired t test was used for statistical analysis. **C**, **D**: Average daily visual acuity of the MA eyes as measured with OKT for WT male mice (**C**, aqua circles), WT female mice (**C**, orange squares), KO male mice (**D**, green triangles), and KO female mice (**D**, purple upside-down triangles). n = 4–6. **E**, **F**: Average daily visual acuity of the LA eyes as measured with OKT for WT male mice (**E**, aqua circles), WT female mice (**E**, orange squares), KO male mice (**F**, green triangles), and KO female mice (**F**, purple upside-down triangles). n = 4–6. **G**, **H**: Average daily visual acuity measurements of the MA eyes (**G**) and the LA eyes (**H**) as measured with OKT for the WT mice (blue circles) and the KO mice (red squares) with male and female mice combined. n = 10–12. **C**–**H**: Error bars represent standard error of the mean (SEM). *p<0.05, **p<0.005, and ***p<0.001 by the linear mixed-effects model.

for each genotype. Consistent with the exacerbation of motor dysfunction (Figure 1 and [18]), we observed a statistically significant exacerbation of the visual acuity deficits in the MA eyes of the Nrf2 KO mice compared with the WT mice (Figure 3G) but did not document any differences in the LA eyes between the two genotypes (Figure 3H).

Nrf2-deficient mice exhibit more severe inflammation of the optic nerve: The optic nerves were harvested and paraffin-embedded at 21 DPI. Two longitudinal sections (corresponding to the medial and lateral nerve) were H&E-stained, scored for inflammatory infiltrates on a scale of 0–3 (where 0 is healthy and 3 is severely inflamed), and averaged to represent each nerve (Figures 4A,B). The Nrf2 KO mice exhibited more severe inflammation of the optic nerve compared with the WT mice (Figure 4A). When the H&E-assessed inflammation of the optic nerve severity was compared with the OKT data (represented as the area under the curve [AUC] throughout the study) for the corresponding eye, the WT mice exhibited the expected correlation such that the higher the inflammation of the optic nerve, the lower the OKT AUC (Figure 4B, blue). Surprisingly, this correlation between inflammation and OKT did not exist in the Nrf2 KO mice (Figure 4B, red). To determine the identity of these inflammatory infiltrates, sections neighboring the H&E-stained optic nerve sections were processed for immunohistochemical analysis with cell type–specific antibodies (Figure 4C–F and Appendix 1). Compared with the healthy, non-EAE optic nerves, the WT and KO EAE optic nerves displayed increased infiltration of T-cells (CD3), macrophages/microglia (Iba1), and B-cells (B220), as well as increased demyelination (CNPase; Figure 4C–F, respectively). Notably, there were no statistically significant differences between the genotypes for the levels of infiltrates or inflammation in the healthy, non-EAE optic nerves, and these data were therefore pooled for the graphs in Figure 4C–F. In contrast, the presence of T-cells, macrophages/microglia, and demyelination (Figure 4C,D,F) was increased in the Nrf2 KO EAE optic nerves compared with the WT EAE nerves with the most statistically significant difference in the $CD3^+$ T-cell infiltration (Figure 4C).

Nrf2-deficient mice lose statistically significantly more RGCs in response to EAE compared with WT mice: To assess neurodegeneration, the retinas were isolated, flatmounted, and stained with the RGC-specific antibody anti-Brn3a at 21 DPI. RGCs were counted in 12 representative fields throughout the retina such that four fields were assessed in the peripheral, medial, and central retina, as described previously [7]. We first established that the healthy, non-EAE Nrf2 KO and WT mice had similar numbers of RGCs before EAE challenge (Figure 5A). In response to EAE, the KO and WT mice exhibited a statistically significant loss of RGCs in all three retinal areas (peripheral, medial, and central; Figure 5B, gray significance indicators), and notably, the Nrf2 KO mice exhibited exacerbated medial and central RGC loss compared with their WT counterparts (Figure 5B). We observed a statistically significant correlation between total RGCs and visual acuity (measured as the AUC of the OKT) in the WT mice such that the eyes with more RGCs exhibited higher visual acuity, but this relation did not exist in the Nrf2 KO mice (Figure 5C). These seemingly paradoxical findings are consistent with the inflammation of the optic nerve results for the Nrf2 KO strain (Figure 4B).

DISCUSSION

The present study was undertaken to determine the consequences of Nrf2 loss for EAE-induced optic neuritis and visual function. The rationale for pursuing this avenue of investigation was twofold. First, mice genetically ablated for Nrf2 were reported to undergo more severe motor deficits following EAE induction [18], and we sought to establish whether this phenomenon extended to the visual deficits that accompany disease onset and progression. Second, the recently approved pharmacological intervention for MS, dimethyl fumarate, is reportedly an Nrf2 activator [10], but the intervention's efficacy in reducing the frequency and/or severity of MS-associated optic neuritis remains to be established. Determining the contribution of Nrf2 to preserving visual function is therefore a key first step toward this goal. The results show that parallel to the motor deficit profiles (Figure 1 and [18]), EAE mice deficient for Nrf2 exhibit exacerbated visual pathology compared with their WT counterparts. We have shown this using the metrics of visual acuity, as measured with OKT, as well as inflammation of the optic nerve and retinal neurodegeneration using immunohistochemical analyses. Interestingly, the data for EAE-associated motor dysfunction conflict with previous reports [18,20], as we consistently observed exacerbated motor deficits in the C57Bl/6J background male mice compared with the female mice. This difference in results may be due to differences in EAE induction protocols, microflora in mice colonies, or other variables that change disease progression. However, the present results are consistent with several human MS studies that reported more progressive disease course in men compared with women [21-23].

An intriguing aspect of the results is that the motor and visual pathologies in EAE differ significantly. Similar to our previous study that used passive transfer models of EAE [7], the motor deficits are progressive and symmetric (Figure 1)

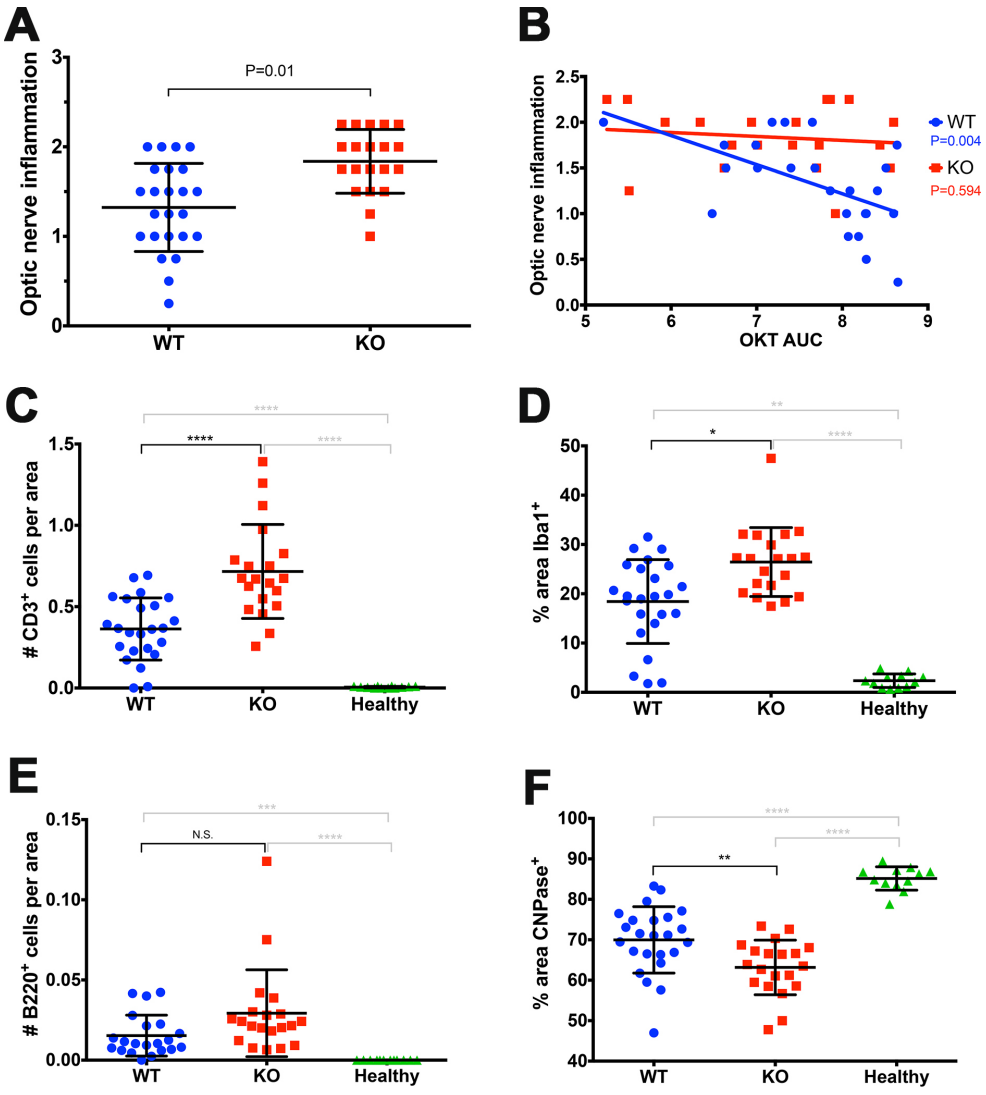

Figure 4. Nrf2-deficient EAE mice exhibit more severe inflammation of the optic nerve and demyelination. **A**: Hematoxylin and eosin (H&E)-stained, paraffin-embedded optic nerves from wild-type (WT; blue circles) or knockout (KO; red squares) experimental autoimmune encephalomyelitis (EAE) mice were scored on a scale of 0–3 for inflammation. Analyzed with the linear mixed-effects model. **B**: Linear regression analysis between inflammation of the optic nerve and area under the curve (AUC) of visual acuity for the corresponding eye as measured with optokinetic tracking (OKT) throughout the study. **C**–**F**: Immunohistochemical analysis and quantitation of paraffin-embedded optic nerves from WT EAE (blue circles), KO EAE (red squares), and healthy, non-EAE (green triangle) mice. T-cells (**C**) and B-cells (**E**) were quantified as the number of $CD3^+$ and $B220^+$ cells, respectively, normalized to the area of the optic nerve. Macrophages (**D**) and myelin (**F**) were quantified as the percentage of the area of nerve positive for Iba1 and CNPase, respectively. **C**–**F**: *p<0.05, **p<0.005, ***p<0.001, and ****p<0.0001 with ordinary one-way ANOVA with either Holmes-Sidak's multiple comparison test. (MCT; **C**, **F**) or Kruskal–Wallis analysis with Dunn's MCT (**D**, **E**). **A**–**F**: n = 24 eyes from 12 WT EAE mice, n = 20 eyes from ten KO EAE mice, and n = 12 eyes from six healthy mice (WT and KO included). Two slides per optic nerve were averaged to represent one point per nerve. Three representative pictures were quantified throughout each slide.

whereas the visual acuity deficits tended to be asymmetric and episodic (Figure 3). Moreover, we observed that the motor deficits were sexually dimorphic (Figure 1) whereas the visual pathology was indistinguishable between genders (Figure 3). These observations suggest that unique mechanisms govern the somatic and visual aspects of EAE and that the underlying mechanism(s) may well be attributable to the established roles for sex hormones in motor function but not vision [24-26].

The EAE results for the WT mice indicate that visual acuity is negatively correlated to inflammation of the optic nerve (Figure 4) and RGC loss (Figure 5), suggesting that one or both are causal factors in functional vision loss. However, to our surprise, this correlation was not retained in the Nrf2 KO EAE mice; visual acuity was not statistically significantly correlated with inflammation of the optic nerve (Figure 4) or with RGC loss (Figure 5). Specifically, we observed that although the Nrf2 KO mice consistently exhibited a statistically significantly more affected eye in terms of visual acuity, the corresponding less affected eye also lost a statistically significant number of RGCs (Figure 5C; depicted by the bottom right red population of points that represent eyes that statistically significantly lost RGCs but not visual acuity). These results show that inflammation of the optic nerve and/or RGC loss is not always linked with visual acuity deficits in EAE. Furthermore, these findings may provide mechanistic

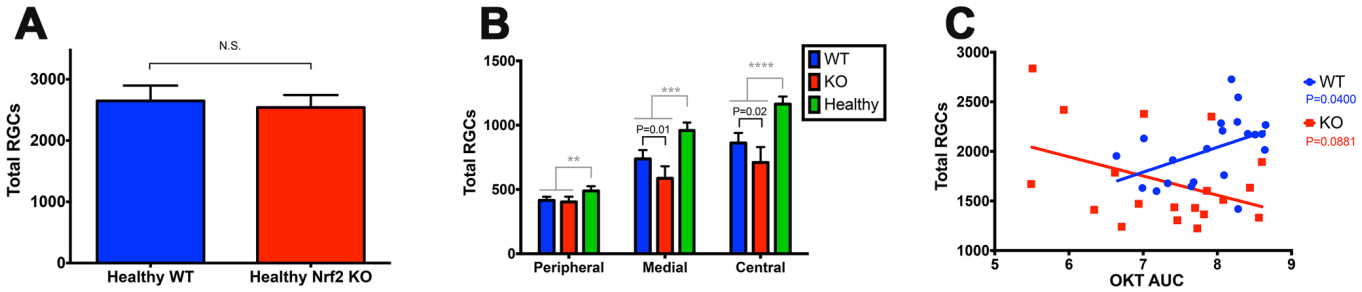

Figure 5. Nrf2-deficient mice exhibit more severe RGC death in central and medial retinas. **A**: Healthy, non-experimental autoimmune encephalomyelitis (EAE) retinal ganglion cell (RGC) counts establishing that 11-week-old, unchallenged wild-type (WT) and Nrf2 knockout (KO) mice do not differ in number of RGCs. Error bars represent standard deviation. n = 12 eyes from six WT mice, and n = 6 eyes from three KO mice. Unpaired two-tailed t test was used for statistical analysis. **B**: Average total regional RGCs counted in both eyes of each EAE mouse at 21 days post-immunization (DPI) for WT (blue left bars), nuclear factor-E2-related factor (Nrf2) KO (red middle bars), and healthy, age-, and strain-matched control mice (green right bars). n = 18–21 eyes from nine to 11 mice per group. Error bars represent standard error of the mean (SEM). **p<0.005, ***p<0.001, and ****p<0.0001 with the linear mixed-effects model. **C**: Linear regression analysis between the total RGCs and the corresponding area under the curve (AUC) of visual acuity as measured with optokinetic tracking (OKT) throughout the study.

insights into patients with MS who do not experience acute visual dysfunction but still experience thinning of the RGC axon layer (the retinal nerve fiber layer) [3].

A caveat of our experimental system is that our studies used global Nrf2 knockouts, and thus, the development of the immune system of WT versus KO mice may be inherently different, which could explain the exacerbated presentation and response to EAE in the KO mice. To address this caveat, we compared the baseline immune profiles of the WT and KO mice before EAE challenge (Figure 2A–C). The results showed that the immune systems of the two strains develop comparably (Figure 2A–C). We appreciate that there may exist a specialized immune cell population(s) that differs between the two genotypes, but based on the data we collected from the unchallenged mice combined with the increased splenic IFN-γ in the Nrf2 KO EAE mice (Figure 2F), we speculate that genotypic differences in immune cell secretion profiles, with a specific amplification of the T-helper 1 (Th1) response, contribute to the increased severity of optical sequelae in mice lacking Nrf2 expression.

In summary, we have determined that mice lacking the cytoprotective transcription factor Nrf2 undergo increased optic neuritis and visual deficits in a murine model of multiple sclerosis. These findings corroborate the amplified motor deficits reported for Nrf2 KO mice and suggest that the recently approved MS treatment, DMF, may have clinical efficacy in limiting visual pathologies for patients.

APPENDIX 1: QUANTITATION METHOD FOR CELL TYPE-SPECIFIC ANTIBODIES IN OPTIC NERVES.

Representative photomicrographs of optic nerves from healthy non-EAE control, WT EAE, and Nrf2 KO EAE mice. CNPase (myelin marker) and Iba1 (macrophage/microglia marker) signal were quantified as % area positive for staining normalized to the area of optic nerve measured. Cells positive for CD3 (T-cell marker) and B220 (B-cell marker) were counted and normalized to area of optic nerve in the picture. Each data point represents the average signal from a medial and lateral section of optic nerve, each with 3 representative fields measured (6 total fields quantified per point). To access the table, click or select the words "Appendix 1."

ACKNOWLEDGMENTS

Scott M. Plafker (plafkers@omrf.org) and Robert C. Axtell (axtellb@omrf.org) are co-corresponding authors on this manuscript. This work was supported by National Institutes of Health Grant R21EY0266684 (SMP), a grant from The Oklahoma Center for the Advancement of Science and Technology (SMP), National Institutes of Health training grant T32 EY023202 (CML), a grant from the Presbyterian Health Foundation (SMP), intramural funds (RCA), and a Nathan Shock Center Grant P30AG050911 (JDW). The content of this manuscript is solely the responsibility of the authors and does not necessarily represent the official views of the National Institutes of Health. We would like to give a special thanks to Dr. Michelle Ratliff and Dr. Carol Webb for providing antibodies and assistance for the flow cytometric analysis of immune organs. A portion of this work was presented

by CML at XXII World Congress of Neurology meeting in Santiago, Chile on November 4, 2015.

REFERENCES

1. Sorensen TL, Frederiksen JL, Bronnum-Hansen H, Petersen HC. Optic neuritis as onset manifestation of multiple sclerosis: a nationwide, long-term survey. Neurology 1999; 53:473-8. [PMID: 10449106].
2. Kaur P, Bennett JL. Optic neuritis and the neuro-ophthalmology of multiple sclerosis. Int Rev Neurobiol 2007; 79:633-63. [PMID: 17531862].
3. Fjeldstad C, Bemben M, Pardo G. Reduced retinal nerve fiber layer and macular thickness in patients with multiple sclerosis with no history of optic neuritis identified by the use of spectral domain high-definition optical coherence tomography. J Clin Neurosci 2011; 18:1469-72. [PMID: 21917458].
4. Henderson AP, Trip SA, Schlottmann PG, Altmann DR, Garway-Heath DF, Plant GT, Miller DH. An investigation of the retinal nerve fibre layer in progressive multiple sclerosis using optical coherence tomography. Brain 2008; 131:277-87. [PMID: 18056739].
5. Gold R, Linington C, Lassmann H. Understanding pathogenesis and therapy of multiple sclerosis via animal models: 70 years of merits and culprits in experimental autoimmune encephalomyelitis research. Brain 2006; 129:1953-71. [PMID: 16632554].
6. Li B, Cui W, Liu J, Li R, Liu Q, Xie XH, Ge XL, Zhang J, Song XJ, Wang Y, Guo L. Sulforaphane ameliorates the development of experimental autoimmune encephalomyelitis by antagonizing oxidative stress and Th17-related inflammation in mice. Exp Neurol 2013; 250:239-49. [PMID: 24120440].
7. Larabee CM, Hu Y, Desai S, Georgescu C, Wren JD, Axtell RC, Plafker SM. Myelin-specific Th17 cells induce severe relapsing optic neuritis with irreversible loss of retinal ganglion cells in C57BL/6 mice. Mol Vis 2016; 22:332-41. [PMID: 27122964].
8. Quinn TA, Dutt M, Shindler KS. Optic neuritis and retinal ganglion cell loss in a chronic murine model of multiple sclerosis. Front Neurol 2011; 2:50-[PMID: 21852980].
9. Lee JM, Johnson JA. An important role of Nrf2-ARE pathway in the cellular defense mechanism. J Biochem Mol Biol 2004; 37:139-43. [PMID: 15469687].
10. Linker RA, Lee DH, Ryan S, van Dam AM, Conrad R, Bista P, Zeng W, Hronowsky X, Buko A, Chollate S, Ellrichmann G, Bruck W, Dawson K, Goelz S, Wiese S, Scannevin RH, Lukashev M, Gold R. Fumaric acid esters exert neuroprotective effects in neuroinflammation via activation of the Nrf2 antioxidant pathway. Brain 2011; 134:678-92. [PMID: 21354971].
11. Gilgun-Sherki Y, Melamed E, Offen D. The role of oxidative stress in the pathogenesis of multiple sclerosis: the need for effective antioxidant therapy. J Neurol 2004; 251:261-8. [PMID: 15015004].
12. Chan K, Lu R, Chang JC, Kan YW. NRF2, a member of the NFE2 family of transcription factors, is not essential for murine erythropoiesis, growth, and development. Proc Natl Acad Sci USA 1996; 93:13943-8. [PMID: 8943040].
13. Zhao Z, Chen Y, Wang J, Sternberg P, Freeman ML, Grossniklaus HE, Cai J. Age-related retinopathy in NRF2-deficient mice. PLoS One 2011; 6:e19456-[PMID: 21559389].
14. Prusky GT, Alam NM, Beekman S, Douglas RM. Rapid quantification of adult and developing mouse spatial vision using a virtual optomotor system. Invest Ophthalmol Vis Sci 2004; 45:4611-6. [PMID: 15557474].
15. Laird NM, Ware JH. Random-effects models for longitudinal data. Biometrics 1982; 38:963-74. [PMID: 7168798].
16. Lindstrom ML, Bates DM. Nonlinear mixed effects models for repeated measures data. Biometrics 1990; 46:673-87. [PMID: 2242409].
17. Axtell RC, de Jong BA, Boniface K, van der Voort LF, Bhat R, De Sarno P, Naves R, Han M, Zhong F, Castellanos JG, Mair R, Christakos A, Kolkowitz I, Katz L, Killestein J, Polman CH, de Waal Malefyt R, Steinman L, Raman C. T helper type 1 and 17 cells determine efficacy of interferon-beta in multiple sclerosis and experimental encephalomyelitis. Nat Med 2010; 16:406-12. [PMID: 20348925].
18. Johnson DA, Amirahmadi S, Ward C, Fabry Z, Johnson JA. The absence of the pro-antioxidant transcription factor Nrf2 exacerbates experimental autoimmune encephalomyelitis. Toxicol Sci 2010; 114:237-46. [PMID: 19910389].
19. Axtell RC, Raman C, Steinman L. Type I interferons: beneficial in Th1 and detrimental in Th17 autoimmunity. Clin Rev Allergy Immunol 2013; 44:114-20. [PMID: 22231516].
20. Okuda Y, Okuda M, Bernard CC. Gender does not influence the susceptibility of C57BL/6 mice to develop chronic experimental autoimmune encephalomyelitis induced by myelin oligodendrocyte glycoprotein. Immunol Lett 2002; 81:25-9. [PMID: 11841842].
21. Rizzo MA, Hadjimichael OC, Preiningerova J, Vollmer TL. Prevalence and treatment of spasticity reported by multiple sclerosis patients. Mult Scler 2004; 10:589-95. [PMID: 15471378].
22. Koch M, Kingwell E, Rieckmann P, Tremlett H, Neurologists UMC. The natural history of secondary progressive multiple sclerosis. J Neurol Neurosurg Psychiatry 2010; 81:1039-43. [PMID: 20639385].
23. Nicot A. Gender and sex hormones in multiple sclerosis pathology and therapy. Front Biosci (Landmark Ed) 2009; 14:4477-515. [PMID: 19273365].
24. Epting LK, Overman WH. Sex-sensitive tasks in men and women: a search for performance fluctuations across the menstrual cycle. Behav Neurosci 1998; 112:1304-17. [PMID: 9926814].
25. Hampson E, Kimura D. Reciprocal effects of hormonal fluctuations on human motor and perceptual-spatial skills. Behav Neurosci 1988; 102:456-9. [PMID: 3395456].

26. Watson NV, Kimura D. Nontrivial Sex-Differences in Throwing and Intercepting - Relation to Psychometrically-Defined Spatial Functions. Pers Individ Dif 1991; 12:375-85.
.

Articles are provided courtesy of Emory University and the Zhongshan Ophthalmic Center, Sun Yat-sen University, P.R. China. The print version of this article was created on 30 December 2016. This reflects all typographical corrections and errata to the article through that date. Details of any changes may be found in the online version of the article.